ON-ORBIT MEASUREMENT OF THE FOCAL LENGTH OF THE SNPP VIIRS INSTRUMENT

James C. Tilton[1], Robert E. Wolfe[1], Guoqing (Gary) Lin[2] and Zhangshi (Albert) Yin[2]

[1]NASA Goddard Space Flight Center, Greenbelt, MD, USA
[2]Science Systems and Applications, Inc., Lanham, MD, USA

ABSTRACT

The Visible Infrared Imaging Radiometer Suite (VIIRS) instrument is a whiskbroom system with 22 spectral bands split between 16 moderate resolution bands (M-bands), five imagery resolution bands (I-bands) and a panchromatic day-night band. Latitude and Longitude geolocation data are generated for each pixel at the M-band, I-band and day-night band spatial resolutions based upon various instrument parameters including focal length. In this study we measure the focal length of the VIIRS instrument from on-orbit data. This is achieved by simulating VIIRS band I2 using Landsat 8 OLI band 5 utilizing the VIIRS instrument system point spread function (PSF) and geolocation data generated with varying values of focal length. The focal length value that produces the highest spatial correlation between the original and simulated VIIRS data is taken to be the measured instrument focal length.

Index Terms—Satellite navigation systems, image registration, image analysis.

1. INTRODUCTION

The NASA/NOAA Visible Infrared Imaging Radiometer Suite (VIIRS) instrument onboard the Suomi National Polar-orbiting Partnership (SNPP) satellite was launched on 28 October 2011. A detailed description of this instrument and its early on-orbit performance is provided in [1]. VIIRS has 5 imagery resolution bands (bands I1 to I5) with 32 detectors each, 16 moderate resolution bands (bands M1 to M16) and a panchromatic day-night band (DNB) with 16 detectors each. In this study we measure the focal length of the VIIRS instrument from on-orbit data.

SNPP VIIRS instrument geometric performance has been calibrated and characterized before launch [2] and on orbit [3, 4]. On-orbit geolocation error detection and correction are based on the results of a ground control point matching (CPM) program [5]. The method described in this paper is similar to the CPM program with emphasis on the variation of cross-correlation coefficients on the focal length. The measured focal length will be used in lookup tables in the ground processing for more accurate geolocation. It also affects scan-to-scan overlap or underlap [6]: the potential issue of that overlap motivated this study.

In the following sections we provide a more detailed description of the imagery resolution data obtained from the VIIRS instrument, describe our method of simulating VIIRS data from Landsat 8 OLI data, and how we use cross correlation to evaluate the quality of this simulation. We then describe how we use these techniques to measure the focal length of the SNPP VIIRS instrument from data collected on-orbit.

2. DESCRIPTION OF VIIRS IMAGERY RESOLUTION DATA

Each cross track scan of the VIIRS instrument's rotating telescope collects data from 32 detectors for each of the five I-bands. These detectors are rectangular with the smaller dimension in the along scan direction. A sample aggregation scheme is employed to equalize the along-scan size of the recorded image sample. In the zone from nadir out to ±31.72° (columns 2017 through 4384) three samples are averaged or aggregated along the scan direction, 31.72° to 44.86° out from nadir (columns 1281 through 2016 and columns 4385 through 5120) two samples are aggregated, and outwards from 44.86° (columns 1 through 1280 and columns 5121 through 6400) no aggregation is employed. These three zones are called the "3x1 aggregation," "2x1 aggregation," and "no aggregation" zones, respectively. In the 3x1 aggregation zone the data from all 32 detectors in each I-band array are transmitted to the ground, whereas in the 2x1 aggregation zone the data from first two and last two rows of each cross track scan are deleted before the data is transmitted to the ground, and in the no aggregation zone the data from the first four and last four rows of each cross track scan are deleted. This data deletion scheme is called "bow-tie deletion." These sample aggregation and bow-tie deletion schemes are unique to the VIIRS instrument. While the sample aggregation scheme should not affect the measured focal length, we intend to later verify this assumption by making measurements in each aggregation zone.

3. SIMULATION OF VIIRS DATA FROM LANDSAT 8 OLI DATA

A key aspect of our approach to measuring the focal length of the VIIRS instrument from on-orbit data is the simulation of VIIRS data from Landsat 8 OLI data. The accuracy of this simulation depends on accuracy of the VIIRS geolocation data. We can evaluate the accuracy of the simulation by cross correlating the simulated and original VIIRS data.

In our experience VIIRS imagery resolution bands I2 and I3 generally provide the finest spatial detail (the atmosphere tends to reduce the visible spatial detail in the other I-bands). We chose to use band I2. The spectral wavelength range for this band (0.85µm – 0.88µm) closely matches that of Landsat 8 OLI band 5. So a sensible choice is to use Landsat 8 OLI band 5 to simulate VIIRS band I2.

The first step of the simulation process is to identify relatively cloud free scenes of VIIRS and Landsat 8 OLI data from the same date that overlap each other spatially and contain locations with distinct spatial features that can be reliably cross correlated on to evaluate the accuracy of the simulation. We have found that locations with numerous small lakes to be ideal. Searching the Landsat and VIIRS archives for such data sets can be a time consuming process. An example of a good pair of VIIRS and Landsat 8 OLI data sets are scenes from 22 July 2016 along the Minnesota and Wisconsin border in the USA (Reflectance_I2 from VIIRS L1B data from year 2016, day 204, UTC 1842 from AS 5000: NPP_VIAES_L1.A2016204.1842.001.2016205034042.hdf, and the Landsat file LC80270282016204LGN00_B5.TIF).

The second step is to select a subset from a particular VIIRS swath that contains a good number of correlatable objects (e.g., small lakes). For I-band data, a swath is 32 rows wide. We could have taken a 32 column by 32 row subset for analysis, but instead took a 128 column by 32 row subset with the thought that the extra columns would provide more correlatable objects to work with. An example of such a subset is from the third swath of the VIIRS data set as shown in Fig. 1.

Fig. 1. An example of a 128 column by 32 row VIIRS subset taken for analysis: Reflectance band I2 at column offset 3888 and row offset 64. The data is from along the Minnesota and Wisconsin border in the USA on 22 July 2016. NOTE: Since this data is from an ascending orbit, south is nominally at the top of this image.

The third step is to convert the VIIRS latitude and longitude coordinates at each VIIRS pixel to UTM_X and UTM_Y coordinates using the pj_transform function from the Cartographic Projections Library (PROJ.4).

The fourth step is to compute the ground sampling distance in the X and Y directions of the VIIRS data by computing the difference of the UTM_X and UTM_Y coordinates in neighboring pixels at the center of the VIIRS image subset. The scale factor between the VIIRS and OLI image data is also calculated in this step as the absolute value of the ratio between the VIIRS and OLI ground sampling distances in each direction. If this scale factor is even, one is added to the scale factor to make the scale factor odd. With an odd scale factor, the center pixel of the grid of OLI pixels associated with each VIIRS pixel corresponds to the center of the VIIRS pixel. For the example subset shown in Fig. 1, the scale factor in the X direction is 15 and the scale factor in the y direction is 13.

The fifth step is to compute the system point spread function (PSF) in the X and Y directions at the scale of the OLI image resampling. The system PSF is triangular in the X (column) direction in the no aggregation zone, and truncated triangular in the 2x1 and 3x1 aggregations zones, with overlap halfway into each pixel on either side. The PSF in the Y (row) direction is rectangular with no overlap. The PSFs for the 3x1 aggregation zone are shown in Fig. 2.

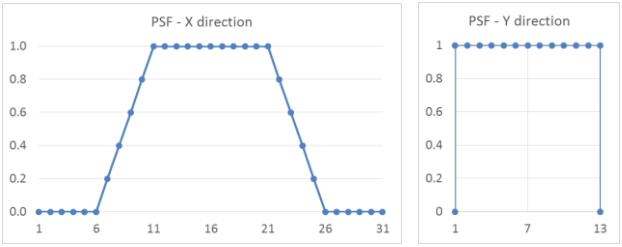

Fig. 2. The VIIRS PSFs in the X and Y directions. With the scale factor equal to 15, the center of the pixel in X direction PSF is at index 16, the center of the pixel to the left is at index 1, and the center of the pixel to the right is at index 31. With the scale factor equal to 13, the center of the pixel in the Y direction PSF is at index 7, and there is no overlap with neighboring pixels.

The simulation is performed in the sixth and final step. For each VIIRS pixel an UTM_X, UTM_Y grid is formed at the nominal Landsat OLI resolution using linear interpolation (in the case of the example data set, this is 29.19m in the X direction and 29.49m in the Y direction). A resampled Landsat OLI subimage is formed for each VIIRS pixel by selecting the nearest neighbor OLI pixel relative to each interpolated grid location. (For the example case, this interpolated grid has 31 columns and 13 rows.) At each VIIRS pixel location, the selected OLI pixels are convolved with the VIIRS PSF to produce the simulated VIIRS pixel value. Fig. 3 shows the resampled Landsat OLI image for the VIIRS subset displayed in Fig. 1, and Fig. 4 shows the simulated VIIRS image.

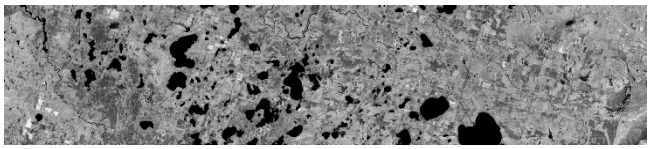

Fig. 3. The resampled Landsat OLI image corresponding to the VIIRS subimage displayed in Fig. 1.

Fig. 4. The simulated VIIRS subset corresponding to the VIIRS subimage displayed in Fig. 1, created by convolving the resampled Landsat OLI image (as in Fig. 3) with the VIIRS PSF (as in Fig. 2).

4. EVALUATION OF SIMULATION QUALITY WITH CROSS CORRELATION

We experimented with evaluation of simulation quality with both normalized mutual information (NMI) correlation and cross correlation. We found that cross correlation gave sharper and stronger peaks. In retrospect we realized that we should have expected this, because there are no contrast reversals between the correlated data sets since they are both produced from measurements in the same wavelength range. (NMI usually only outperforms cross correlation when there are contrast reversals between the compared images.)

To maximize the performance of the cross correlation, we scaled the original and simulated VIIRS imagery to the same range before performing the cross correlation, and maintained the data in floating point format (we did not quantize the data into integer values).

We found that there is often a small offset between the VIIRS and Landsat OLI geolocation, as much as 4 pixels in the Landsat resolution. Taking this into account, we define the cross correlation (*CC*) between the original VIIRS image, *o*, and the simulated VIIRS image, s_{rc}, (where r = the row shift and c = the column shift of the Landsat OLI image), to be:

$$CC = \max_{rc}\left\{\frac{\sum_x\sum_y[o(x,y)-\bar{o}][s_{rc}(x,y)-\overline{s_{rc}}]}{\sqrt{\sum_x\sum_y[o(x,y)-\bar{o}]^2\sum_x\sum_y[s_{rc}(x,y)-\overline{s_{rc}}]^2}}\right\} \quad (1)$$

CC = 0.982 with $r = c = 0$ for the simulated VIIRS subimage displayed in Fig. 4. However, with $r = 2$ and $c = 0$, *CC* = 0.996. The *r* and *c* that we observed are similar to the VIIRS geolocation errors reported in [5].

We assume that *CC* positively correlates with the quality of the VIIRS simulation.

5. REGENERATING VIIRS GEOLOCATION DATA WITH VARYING VALUES OF FOCAL LENGTH

In our preliminary tests we found that a slight decrease in focal length produced an increase in the values of *CC*. For the tests reported here, we regenerated the VIIRS geolocation data for focal length values calculated as a small percentage decrease from the designed focal length value of 0.28525m, as listed in Table I. (The current operationally assumed focal length value is a -0.35% decrease from the designed focal length, or 0.28425m.)

We require VIIRS Level-1B geolocation and reflectance data for our analysis. We regenerated the geolocation data from the available VIIRS Level-1A data, which is available in 6 minute granule boundaries. We used the NASA VIIRS Level-1 software Version 2.0 for our reprocessing with VIIRS Level-1 LUT Version 2.0.0.3, except for variations in the focal length parameter. We also regenerated the VIIRS Level-1B geolocation and reflectance data for the operational focal length value, because this data is not currently available at 6 minute granule boundaries for all dates (this data will be available for all dates once the AS 5000 reprocessing is complete). We note that the reflectance data is not affected by the focal length variations.

6. MEASURING THE FOCAL LENGTH OF THE SNPP VIIRS INSTRUMENT

We now measure the focal length of the SNPP VIIRS instrument by varying the assumed value of the focal length in the ground processing system and regenerating the VIIRS geolocation data. We assume that the correct focal length corresponds to the focal length value that produces the highest value of *CC* (eq. 1). Table I lists the values of *CC* (max at $r = 2$ and $c = 0$) for the example VIIRS subset shown in Fig. 1. A plot of *CC* versus % decrease in focal length is provided in Fig. 5.

As shown in Fig. 5, the plot of *CC* is a very smooth curve that can be very closely fit by a 2nd degree polynomial, as verified by the high R^2 value. (The curve fitting and R^2 value calculation are from the MS Excel scatter plot of the data.) The first derivative of this curve can be solved to find the location of the peak of the curve, which is at -0.525%.

Table I. Focal length values tested.

% decrease	focal length (m)	*CC*
-1.0%	0.28240	0.9963
-0.8%	0.28297	0.9971
-0.6%	0.28354	0.9974
-0.4%	0.28411	0.9973
-0.2%	0.28468	0.9969
0%	0.28525	0.9961

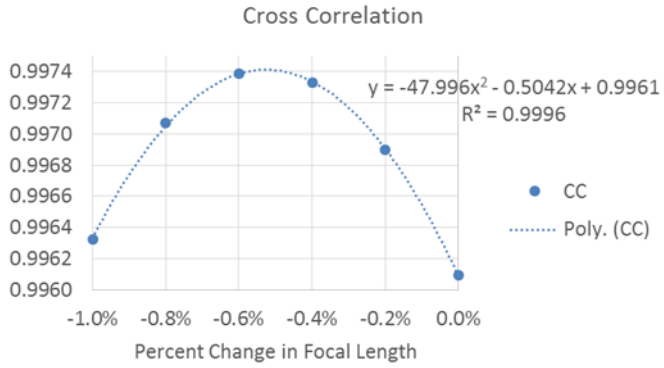

Fig. 5. Plot of *CC* from Table I. The 2nd degree polynomial that best fit the data points is also plotted. The peak of the curve is at -0.525%.

We must perform similar measurements on several other subsets for which high R^2 values and high peak *CC* values are obtained to be able to evaluate the statistical robustness of this approach.

7. RESULTS

We performed the described analysis on 128 column by 32 row subsets of several scans from nineteen VIIRS data sets from dates ranging from 15 August 2013 through 13 November 2016. The analyzed portion of data fell in the 3x1 aggregation zone in twelve data sets, the 2x1 aggregation zone in six data sets, and the no aggregation zone in six data sets (the analyzed portion of some data sets included portions of two aggregation zones).

All but four of the data sets were from an area with many small lakes in the western Great Lakes region of the USA and Canada, including Wisconsin, Northern Michigan, Minnesota and Western Ontario. Three of the data sets were from an area of central Argentina that also has many small lakes, and one data set was from the Victoria state of Australia.

In Table II we list the results from data sets for which the at least a part of analyzed portion fell in the 3x1 aggregation zone, Table III lists results from the 2x1 aggregation zone, and Table IV lists results from the no aggregation zone. All of these results are from data subsets where the fitted curve has a peak ≥ 0.95 and an R^2 value ≥ 0.99.

The measurements from the no aggregation zone generally have higher standard deviation than those from the other two aggregation zones. This is because the pixel resolution in that zone is coarser than the other two zones.

Since the results from the no aggregation zone generally have a noticeably higher standard deviation than the measurements from the other two aggregation zones, we take as our estimate of the VIIRS instrument to be a weighted average of the 3x1 and 2x1 aggregation zone results: a 0.506% decrease from the designed focal length, or 0.28381m.

Table II. Results from twelve data sets in the 3x1 aggregation zone (GL = Great Lakes, DOY = day of year).

Site	Year	DOY	# scans	mean	std. dev.
GL	2013	227	30	-0.525	0.046
GL	2014	143	15	-0.504	0.050
GL	2014	145	17	-0.471	0.088
GL	2015	116	30	-0.482	0.036
GL	2015	196	21	-0.501	0.043
So. Aus.	2015	287	11	-0.504	0.042
Arg.	2015	361	14	-0.510	0.054
GL	2016	103	20	-0.494	0.025
GL	2016	204	19	-0.510	0.044
GL	2016	277	31	-0.535	0.039
GL	2016	309	22	-0.523	0.050
GL	2016	316	25	-0.515	0.034
			Weighted Mean:	-0.508	

Table III. Results from six data sets in the 2x1 aggregation zone (GL = Great Lakes, DOY = day of year). In the scan column, *s* designates start scan and *e* designates end scan.

Site	Year	DOY	# scans	mean	std. dev.
Arg.	2016	55	16*s*	-0.489	0.092
GL	2016	126	8*e*	-0.485	0.056
GL	2016	243e	19*e*	-0.484	0.037
GL	2016	243s	11*s*	-0.509	0.040
GL	2016	277	10*s*	-0.525	0.038
GL	2016	309	11*s*	-0.523	0.045
			Weighted Mean:	-0.500	

Table IV. Results from six data sets in the no aggregation zone (GL = Great Lakes, DOY = day of year). In the scan column, *s* designates start scan and *e* designates end scan.

Site	Year	DOY	# scans	mean	std. dev.
Arg.	2016	21	19*s*	-0.582	0.079
GL	2016	126	15*s*	-0.524	0.091
GL	2016	126	20*e*	-0.506	0.079
GL	2016	243	15*e*	-0.513	0.080
GL	2016	243	22*s*	-0.491	0.040
GL	2016	318	15*s*	-0.497	0.122
			Weighted Mean:	-0.519	

8. CONCLUDING REMARKS

We have described an approach for measuring the focal length of the VIIRS instrument from on-orbit data. We have shown that with suitable pairs of VIIRS and Landsat OLI data sets we can produce high quality measurements of the focal length. This assertion of high quality is supported by very high values (> 0.95) of the cross correlation between the original VIIRS image and VIIRS image simulated from Landsat OLI data, high values of the R^2 values (> 0.99) for the 2nd degree polynomial fit to the cross correlation results at differing focal lengths, and low values (< 0.1%) of the standard deviation of the focal length measurements.

The reported results include measurements from the first four years of operation of the VIIRS instrument. We see no obvious change in the measured focal length during these four years. We also see no discernible difference between measurements in the different aggregation zone, except for a higher standard deviation of the measurements in the no aggregation zone.

9. REFERENCES

[1] C. Cao, F. J. De Luccia, X. Xiong, R. E. Wolfe and F. Weng, "Early on-orbit performance of the visible infrared imaging radiometer suite onboard the Suomi National Polar-Orbiting Partnership (S-NPP) satellite," *IEEE Trans. Geosci. Remote Sens.*, vol. 52, no. 2, pp. 1142-1156, 2014.

[2] G. Lin, R. E. Wolfe and M. Nishihama, "NPP VIIRS geometric performance status," *Proc. SPIE*. 8153, Earth Observing Systems XVI, 81531V (Sept. 13, 2011); doi: 10.1117/12.894652.

[3] R. E. Wolfe, G. Lin, N. Masahiro, K. P. Tewari and E. L. Montano, "NPP VIIRS early on-orbit geometric performance," *Proc. SPIE* 8510, Earth Observing Systems XVII, 85101 (Oct. 15, 2012);.doi: 10.1117/12.929925.

[4] R. E. Wolfe, G. Lin, M. Nishihama, K. P. Tewari, J. C. Tilton and A. R. Isaacman, "Suomi NPP VIIRS prelaunch and on-orbit geometric calibration and characterization", *J. Geophys. Res. Atmos.*, vol. 118, pp. 11,508–11,521, doi:10.1002/jgrd.50873, 2013.

[5] R. E. Wolfe and M. Nishihama, "Accurate MODIS global geolocation through automated ground control image matching," in *Image Registration for Remote Sensing*, J. Le Moigne, N. S. Netanyahu and R. D. Eastman (eds.), Cambridge Univ. Press, New York, pp. 437-455, 2011, doi: 10.1017/cbo9780511777684.022.

[6] G. Lin, R. E. Wolfe and J. C. Tilton, "Trending of SNPP ephemeris and its implications on VIIRS geometric performance," *Proc. of SPIE* 9972, Earth Observing Systems XXI, 99721K (Oct. 5, 2016); doi: 10.1117/12.2239043.